J Mater Sci: Mater Electron (2013) 24:1264–1273
DOI 10.1007/s10854-012-0917-0

Investigation of microstructural, Vickers microhardness and superconducting properties of $YBa_2Cu_{3-x}Gd_xO_{7-\delta}$ ($0 \leq x \leq 0.150$) superconducting ceramics via experimental and theoretical approaches

M. Dogruer · G. Yildirim · O. Ozturk · A. Varilci · N. Soylu · O. Gorur · C. Terzioglu

Received: 17 July 2012 / Accepted: 20 September 2012 / Published online: 29 September 2012

Abstract This study manifests the change of pinning mechanism, electrical, structural, physical, mechanical and superconducting properties of $YBa_2Cu_{3-x}Gd_xO_{7-\delta}$ superconductors samples prepared by the conventional solid-state reaction method (x = 0, 0.025, 0.050, 0.100 and 0.150) by use of dc resistivity, X-ray analysis (XRD), scanning electron microscopy (SEM) and Vickers microhardness measurements. Zero resistivity transition temperatures (T_c^{offset}) of the samples are deduced from the dc resistivity measurements. Additionally, the lattice parameters are determined from XRD measurements when the microstructure, surface morphology and microhardness of the samples studied are examined by SEM and mechanical measurements, respectively. The results obtained demonstrate that T_c^{offset} values of the samples decrease slowly with the increase in the Gd content. The maximum T_c^{offset} (92.0 K) is obtained for the pure sample prepared at 940 °C for 20 h in air atmosphere while the minimum value of 83.3 K is found for the sample doped with 0.150 Gd content. Moreover, it is obtained that J_c values reduce from 132 to 34 A/cm^2 with the enhancement of the Gd level in the crystalline structure. Further, the peak intensities belonging to Y123 (major) phase are obtained to decrease whereas the peak intensities of the minor phases such as $BaCuO_2$ and Y211 are found to enhance systematically with the increment in the Gd content in the system, illustrating that partial substitution of Cu^{2+} ions by Gd^{3+} ions are carried out successfully. Moreover, SEM images display that the undoped sample obtains the best crystallinity and connectivity between superconducting grains and largest grain size whereas the worst surface morphology is observed for the maximum doped sample (x = 0.150). At the same time, Vickers microhardness, elastic modulus, load independent hardness, yield strength, fracture toughness and brittleness index values, playing important roles on the mechanical properties, are computed for all the samples. The experimental results of the microhardness measurements are examined using the Meyer's law, PSR (proportional specimen resistance), modified PRS, Elastic–Plastic deformation model (EPD) and Hays–Kendall (HK) approach. The microhardness values obtained increase with the enhancement of the Gd content in the samples. Besides, it is noted that the Hays–Kendall approach is the most successful model explaining the mechanical properties of the samples studied in this work.

M. Dogruer (✉) · G. Yildirim · A. Varilci · N. Soylu · O. Gorur · C. Terzioglu
Department of Physics, Abant Izzet Baysal University, 14280 Bolu, Turkey
e-mail: musadoqruer@gmail.com

O. Ozturk
Department of Physics, Kastamonu University, 37100 Kastamonu, Turkey

1 Introduction

Since the discovery of high-T_c superconductor $YBa_2Cu_3O_{7-x}$ (Y123) with critical transition temperature above 77 K [1], the interest in applications in technology and industry of these materials has been increased day by day. However, the applied magnetic fields and high temperatures limit their applications due to the presence of grain and sub-grain boundaries in the materials [2–4]. Hence, several techniques have been used to improve the superconducting, electrical, mechanical, physical, microstructural and flux pinning properties of the superconductor materials to make them suitable for high temperature and magnetic field applications [5, 6].

As well known from the literature, critical current density, being responsible for these applications, is inadequately low in the YBaCuO superconducting materials because of the weak links and the granularity in these materials [7]. Consequently in the last decades, several methods including the chemical doping or substitution, transition metal evaporation and changing preparation condition (time, temperature, atmosphere, pressure) have been examined to make the effective pinning centers such as planar defects, stacking faults and micro-defects, leading to the improvement of the critical current density and critical transition temperature [8–10]. The chemical substitution is one of the most preferred methods owing to easily controllable mechanism and the reproducible process [11–13]. Moreover, the knowledge of both the location and charge of the doping metals allows us to obtain some important clues about the degradation or improvement of the superconducting properties (hole carrier concentration, critical current density, onset and offset critical temperatures, etc.) [14]. Therefore, this method is useful to investigate the mechanism of high-temperature superconductivity [15–19].

In the present work, we report the role of partial replacement of Cu^{2+} ions by Gd^{+3} ions on electrical, structural, physical, mechanical and superconducting properties of $YBa_2Cu_{3-x}Gd_xO_{7-\delta}$ superconductor samples prepared by the conventional solid-state reaction method with the aid of the XRD, SEM, H_v, ρ–T and I–V measurements. Moreover, the results of the microhardness measurements are analyzed using the different models such as Meyer's law, PSR, MPRS, EPD and HK approach. The results obtained demonstrate that the partial substitution of Cu^{2+} ions by Gd^{+3} ions in the Y123 system leads to not only the decrement of the critical transition temperature and current density but the induction of an orthorhombic–tetragonal phase transition and the degradation of the surface morphology and grain connectivity, as well [20, 21].

1.1 Experimental details

In this study, samples with the nominal stoichiometry of $YBa_2Cu_{3-x}Gd_xO_{7-\delta}$ ($0 \leq x \leq 0.150$) are elaborated in air by conventional solid-state reaction. Starting materials Y_2O_3, CuO, $BaCO_3$ and Gd_2O_3 (Alfa Aesar Co., Ltd. 99.9 % purity) are mixed in a grinding machine for 24 h until the mixture becomes blackish in color. The homogeneous mixture of powders is exposed to calcination process in alumina crucible at 900 °C for 20 h in a tube furnace (Protherm-Model PTF12/75/200) at 5 °C/min heating rate in air with an intermediate grinding. The resultant powder (homogeneous black product) is pressed into rectangular bars with dimensions of $10 \times 4 \times 2$ mm^3 by applying a load of 300 MPa at the room temperature. The bars obtained are annealed in the tube furnace with 5 °C/min heating rate at 940 °C for 20 h in air atmosphere. Then, the bars are left in the furnace to cool down to approximately 700 °C below which the sintering process of the samples is carried out in oxygen atmosphere. In the current work, the undoped sample is denoted as Gd0 while the Gd substituted $YBa_2Cu_{3-x}Gd_xO_{7-\delta}$ superconductors produced by various content such as 0.025, 0.050, 0.100 and 0.150 will be herein after denoted as Gd1, Gd2, Gd3 and Gd4, respectively.

Dc resistivity is measured using A Keithley 220 programmable current source and a Keithley 2182A nano-voltmeter. Moreover, the transport critical current experiments of the samples in self-field are measured by home-made system at 77 K in zero field by means of the four-probe method. A programmable temperature controller (Lakeshore 340) is used for the accurate monitoring of the temperature with a stability and accuracy of ±0.01 K. All the data taken are recorded using the Labview computer software.

In addition, X-ray diffraction measurements were performed using a Rigaku Multiflex + XRD diffractometer with CuK_α target giving a monochromatic beam with wavelength 1.5418 Å in the range $2\theta = 3$–60° at a scan speed of 3°/min and step increment of 0.02° at room temperature (300 K). The lattice parameters, phase structures and impurities for the samples are deduced from the XRD patterns. The accuracy in determining the lattice parameters (a, b and c) is found to be ±0.0001.

Moreover, the grain connectivity and surface morphology of the samples are identified using a Jeol scanning electron microscope (SEM) JEOL 6390-LV, operated at 20 kV, with a resolution power of 3 nm.

Hardness measurements of $YBa_2Cu_{3-x}Gd_xO_{7-\delta}$ samples are performed on the polished surface of the examined samples with the aid of a digital microhardness tester (Instron Series 2100) at room temperature. The applied load (F) is varied from 0.245 to 2.940 N and the applied time is 10 s for all trials, and the diagonals of indentation are measured with an accuracy of ±0.1 μm. Indentations are made at different parts of the samples' surface in such a way that the distance between any two indentations is not less than two times the diagonal of the indentation mark to avoid surface effects due to neighboring indentation. An average of 5 readings at different locations of the specimen surfaces is taken to obtain reasonable mean values for each load.

2 Result and discussion

2.1 Electrical resistivity measurements

We conducted the dc electrical resistivity measurements as a function of temperature to examine the effect on

superconducting properties of Gd content in the Y123 system. The electrical resistivity is measured by running the dc current of 5 mA through the bulk surface with the aid of the standard four-probe dc technique in the temperature range of 80–100 K in the cryostat and the resistivity results obtained are displayed in Fig. 1. It is observed that all the samples show metallic behavior above the T_c value. The normal state resistivity is observed to regularly enhance with ascending the Gd content to a maximum value of 3.39 mΩ cm for x = 0.15 as against 1.31 mΩ cm for the Gd0 sample (Table 1). When Gd^{3+} ions are substituted by Cu^{2+} in the Y-123 system, each doping of Gd^{3+} fills one hole in the crystal, leading to decrement in the hole concentration in the Cu–O plane of the system, and thus an increment of normal-state resistivity of the Y123 system is observed. With the increase of the Gd^{3+} ions in the system the normal-state resistivity enhances continuously [22, 23]. Moreover, the onset critical (T_c^{onset}) and offset critical (T_c^{offset}) temperatures inferred from the normalized resistivity graphs are depicted in Table 1. It is visible from the table that both the T_c^{onset} and T_c^{offset} values degrade systematically with the increment of the Gd content in the system as a result of the enhancement in the relative percentage of Y-211 phase formation, and especially the reduction of the mobile carrier concentration. The maximum T_c^{onset} of 95.2 K and T_c^{offset} of 92.0 K are observed for the Gd0 sample while the Gd4 sample obtains the smallest values (Table 1) as a consequence of the presence of impurities and weak links between the superconducting grains [24], being favored by the SEM investigations.

2.2 XRD analyses

Figure 2 indicates the room temperature powder X-ray diffraction (XRD) patterns between 20° and 60° for the $YBa_2Cu_{3-x}Gd_xO_{7-\delta}$ superconductor materials with x = 0, 0.025, 0.050, 0.100 and 0.150. The diffraction patterns obtained are used to determine the texture, grain size, interplaner distance and lattice constant parameters of the pure and Gd-doped samples. Characteristic peaks corresponding to the different phases such as Y123 (major), $BaCuO_2$ and Y211 (minor) are marked on the patterns. The XRD analysis indicates that all the samples mainly are composed of perovskite based Y123 phase with an orthorhombic Pmmm symmetry. Hence, the peaks shown are indexed on the basis of Y123 (major phase) structure (Fig. 2). Further, one can see from figure that all the samples prepared exhibit the polycrystalline superconducting phase with less intensity of diffraction lines as the Gd

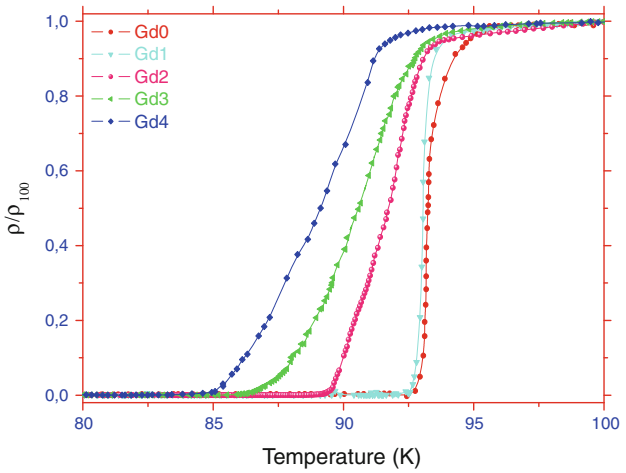

Fig. 1 Normalized resistivity as a function of temperature curves for Gd0, Gd1, Gd2, Gd3 and Gd4

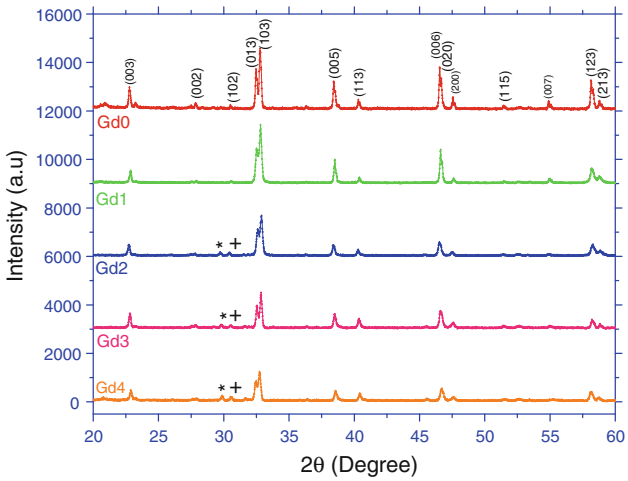

Fig. 2 XRD patterns of Gd0, Gd1, Gd2, Gd3 and Gd4 samples

Table 1 Some characteristics of superconducting samples

Samples	T_c^{onset}	T_c^{offset}	$\rho_{300\ K}$ (mΩ cm)	a (Å)	b (Å)	c (Å)	J_c (A cm^{-2})	Grain size (nm)
Gd0	95.2	92.0	1.31	3.816	3.888	11.684	132	58.3
Gd1	95.1	91.5	2.06	3.822	3.886	11.670	108	48.4
Gd2	94.6	89.1	2.90	3.826	3.885	11.674	74	19.2
Gd3	94.4	85.8	3.26	3.821	3.883	11.675	51	18.6
Gd4	93.6	83.3	3.39	3.820	3.882	11.674	34	16.4

Table 2 The calculated load dependent H_v, E, Y, K_{IC} and B for the samples

Samples	H_v (GPa)	E (GPa)	Y (GPa)	K_{ic} (Pa/m$^{1/2}$)	B (μm$^{1/2}$) × 10^{-3}
Gd0	3.866	316.87	1.288	2492	1.55
	3.531	289.41	1.177	2381	1.48
	3.020	247.53	1.000	2202	1.37
	2.719	222.86	0.906	2090	1.30
	2.705	221.71	0.901	2084	1.29
Gd1	4.286	351.30	1.428	2904	1.47
	3.903	319.90	1.301	2772	1.40
	3.385	277.45	1.128	2581	1.31
	2.932	240.32	0.977	2402	1.22
	2.842	232.94	0.947	2365	1.20
Gd2	4.410	361.46	1.470	2919	1.51
	4.011	328.76	1.337	3041	1.31
	3.500	286.87	1.166	2784	1.25
	3.020	247.53	1.006	2639	1.14
	2.984	244.58	0.994	2401	1.24
Gd3	4.500	368.84	1.500	2804	1.60
	4.212	345.23	1.404	2713	1.55
	3.712	304.25	1.237	2546	1.45
	3.315	271.71	1.105	2406	1.37
	3.310	271.30	1.103	2405	1.37
Gd4	4.817	394.82	1.605	2688	1.79
	4.350	356.54	1.450	2554	1.70
	3.910	320.48	1.303	2421	1.61
	3.586	293.92	1.195	2319	1.54
	3.577	293.18	1.192	2316	1.54

content increases in the system. The peak intensities belonging to major phase are obtained to decrease whereas the peak intensities of the minor phases such as $BaCuO_2$ and Y-211 are found to enhance systematically with the increment in the content of the Gd, revealing that why the superconducting proper ties degrade with the enhancement of the Gd doping in the system. In addition, we observe no another phase containing Gd or any other cation in the XRD graphs of the Gd-substituted samples even up to $x = 0.15$, demonstrating that the Gd ions enter into the crystal structure by replacing Cu ions. As for the cell structure of the samples prepared, the lattice parameters *a, b* and *c* are calculated using the least square method through *d* values and (*hkl*) planes for the orthorhombic unit cell structure. The variation of the cell parameters *a*, *b* and *c* evaluated from the XRD graphs of the samples is listed in Table 2. A considerable change in cell parameters of the samples is found within the experimental limit of 0.0001 Å. It is apparent from the table that a systematic elongation in the *a* and *b*-axis lengths is observed due to an increase in the oxygen content in the CuO chains [25, 26] whereas a contraction in the *c*-axis length is obtained with the increase of the Gd content, confirming the incorporation of the Gd^{3+} ions into the structure [27–30]. Moreover, it is well known that the lattice parameter *a*, being controlled by the length of in-plane Cu–O bond may be expanded or contracted with the change of the electrons into antibonding orbital. In the Y123 system the cell parameter *a* is expanded because of the partial replacement of Cu^{2+} ions by Gd^{3+} ions, resulting in both an increase of the lattice parameter a, and a decrease in the c parameter.

2.3 Grain size calculation

As well known the XRD curves allow us to calculate the crystallite size of a superconducting ceramic. According to the broadening nature of the XRD peaks of the ceramic, the particle size can be determined from the Scherrer–Warren equation [31–34].

$$d = {}^{0.941\lambda}/_{B\cos\theta_B} \quad (1)$$

where d denotes the crystal thickness, λ presents the wavelength and B represents the full width at half maximum (FWHM) of the Bragg peak corrected using the corresponding peak in micronized and θ_B is the Bragg angle. Further,

$$B^2 = B_m^2 - B_s^2 \quad (2)$$

where B_s is the half width of the standard material in radians. Based on the calculations performed, the average grain size values (in broadening region) of the samples are found to be within the nanometer scale (Table 1). Moreover, it is another important point deduced from Fig. 2 that the FWHM values reduce with the enhancement of the Gd-content in the system, confirming that the pure sample has the largest grain size and best crystallinity and connectivity between grains [17].

2.4 SEM analyses

The surface morphologies of the $YBa_2Cu_{3-x}Gd_xO_{7-\delta}$ materials produced are examined by scanning electron microscopy (SEM) investigations. We realized that there is a systematic change in the micrographs and thus we give only the micrographs of the Gd0 (the best) and Gd4 (the worst) sample in Fig. 3 to show the main differences between them. Figure 3 displays that the microstructures of the samples studied are found to be surprisingly different from each other. Namely, the grain size of the Gd0 sample is found to be much larger from the Gd4 sample. Likewise, the surface of the former sample is observed to be smoother and denser. Additionally, the sample obtains more uniform surface appearance, better texturing, lower porosity, better

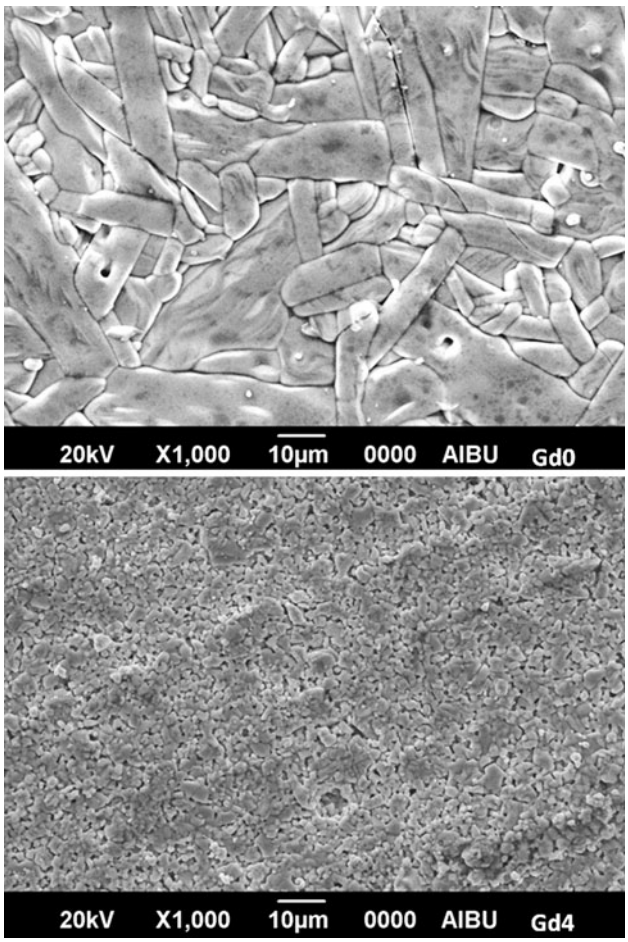

Fig. 3 SEM micrographs Gd0 and Gd4 samples

crystallinity and connectivity between grains compared to the latter one. Based on these results obtained, not only is the microstructure of the Y123 bulk superconductor dependent strongly upon the Gd content but also the grain connectivity and crystallite size degrade as a result of the presence of the Gd^{3+} ions in the Y123 system.

2.5 Transport critical current density

There are several methods to explain the pinning mechanism in the superconducting materials [35–38]. Critical current density (J_c) measurement is one of the most popular. Figure 4 demonstrates the effect of the partial replacement of Cu^{2+} ions by Gd^{+3} ions on the self-field critical current density of the Y123 bulk superconductors. As can be seen from the figure the J_c value of the samples studied reduces with the increment of the Gd content (Table 1). The virgin (Gd0) sample shows a J_c of 132 A/cm^2 (the maximum value) while the minimum J_c is found to be about 34 A/cm^2 for Gd4 sample at 77 K. This decrement in J_c is related to not only the decrease of the flux pinning centers but also the enhancement of the weak links between

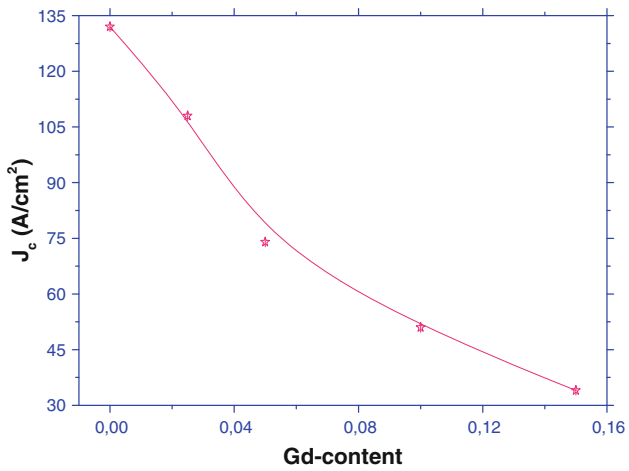

Fig. 4 J_c of pure and Gd-doped samples (the dashed line is a guide for the eyes)

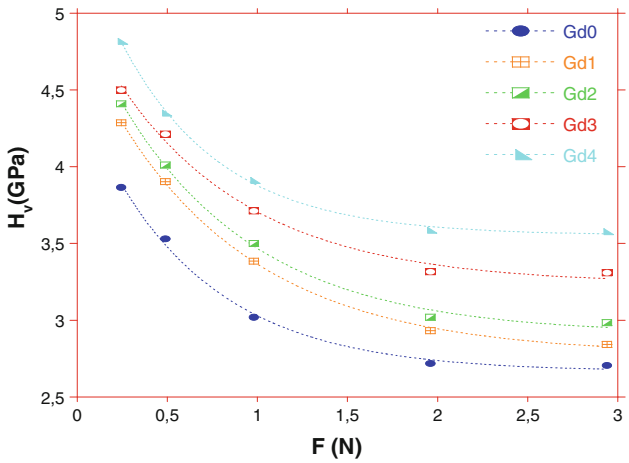

Fig. 5 Variation of load dependent microhardness H_v with applied load F

the superconducting grains, secondary (minor) phases, the micro-deformations, porosity, grain boundaries resistance, and de-orientation of Y123 grains as the Gd content increases in the Y-123 system, supporting the results of the structural investigations [39].

2.6 Microhardness and modeling

Vickers microhardness values (H_v) of the different applied loads ($0.245 \leq F \leq 2.940$) are computed using the following equation:

$$H_V = 1854.4\left(\frac{F}{d^2}\right) \quad (3)$$

where d presents the diagonal length of the indentation. The change of the microhardness with the applied loads on

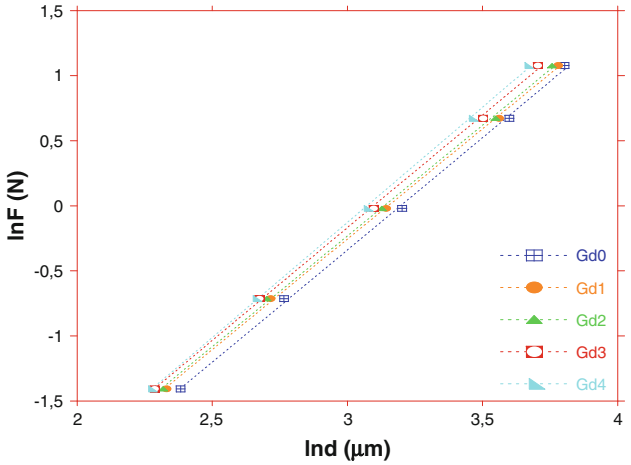

Fig. 6 Variation of applied load *lnF* with diagonal *lnd* for the Samples

the surfaces of the $YBa_2Cu_{3-x}Gd_xO_{7-\delta}$ ($0 \leq x \leq 0.150$), superconducting ceramics is illustrated in Fig. 5. The Vickers hardness (H_v), elastic modulus (E), yield strength (Y), fracture toughness (K_{IC}) and brittleness index (B) values determined are listed in Table 2. It is obtained from the Table 2 that the microhardness values enhance with ascending the Gd content and the Gd4 sample, among the samples studied, has the highest microhardness values for all the applied loads. In fact, the microhardness value of 3.577 GPa is found to be the maximum for the Gd4 sample whereas the minimum value (2.705 GPa) is obtained for the Gd0 sample in the applied load of 2.940 N. The increase of microhardness value with the increment of the Gd doping can be explained by the formation of impurities, porosities and irregularities as observed in the SEM investigations [40, 41]. The H_v (in GPa unit) value computed reduces rapidly with ascending $F(N)$ up to 2 N and remains approximately constant hereafter. The rapid change of microhardness value is obtained with the enhancement of the applied load in the range from 0.245 to 2.000 N.

The hardness values ascend rapidly as the applied load increases up to 2 N beyond which the curves shift to the saturation (plateau) region, confirming the weak grain boundaries, impurity phases and irregular grain orientation distribution [42]. This behavior is known as indentation size effect (ISE) [43–45]. Dogruer et al. obtained the similar results for the Cu-diffused bulk MgB_2 superconductor samples [33, 46]. Moreover, according to Fig. 5, the H_v values depend strongly on the Gd content in Y123. In literature, several models such as such as Meyer's law, proportional specimen resistance (PSR), modified PRS (MPSR), elastic–plastic deformation model (EPD) and Hays–Kendall (HK) approach are suggested to both compute the load independent microhardness and explain ISE (indentation size effect) clearly [47, 48].

Table 3 Best-fit results of experimental data according to Meyer's Law

Samples	n	lnA (GPa)	H_V (GPa)
Gd0	1.73	−5.53	2.705–2.719
Gd1	1.70	−5.36	2.842–2.932
Gd2	1.70	−5.36	2.984–3.020
Gd3	1.73	−5.38	3.310–3.315
Gd4	1.77	−5.45	3.577–3.586

2.6.1 Analysis using Meyer's law

Meyer's law describes the relation between indentation load (F) and the indentation size (d) [49]:

$$F = Ad^n \tag{4}$$

where power n presents Meyer number, and A denotes the standard hardness constants. Figure 6 shows the plots of lnF versus lnd for all the samples. The slope of the $ln\ F$–$ln\ d$ graph gives n when the vertical intercept signifies A value. The n and A values obtained from the curves are listed in Table 3. As seen from the table, the value of Meyer number randomly changing is found to be less than 2 for the samples produced in this study, confirming that the load dependent displacement is due to the ISE behaviour.

2.6.2 Analysis according to proportional specimen resistance (PSR) model

According to literature, the ISE can be explained as follows [50, 51]:

$$\frac{F}{d} = W + Ad \tag{5}$$

where W gives the surface energy when A presents load independent microhardness value. The hardness value can be obtained from the PSR model with the aid of the following equation:

$$H_{PSR} = 1854.4A \tag{6}$$

Figure 7 displays the variation of F/d versus d for the samples prepared. The W, A and H_{PSR} values calculated are tabulated in Table 4. As seen from the table, the load independent microhardness values ascend with the increment of the Gd doping. Furthermore, according to the PSR model calculation, the H_{PSR} value (2.271 GPa) of the pure (Gd0) sample is found to be lower than the H_v value in the saturated region (2.705 GPa). This behavior is also observed for all the other samples (Gd1, Gd2, Gd3 and Gd4, respectively).

Equations (7–10) and load independent H_{PSR} are used to calculate the load independent elastic modulus (E_0), yield

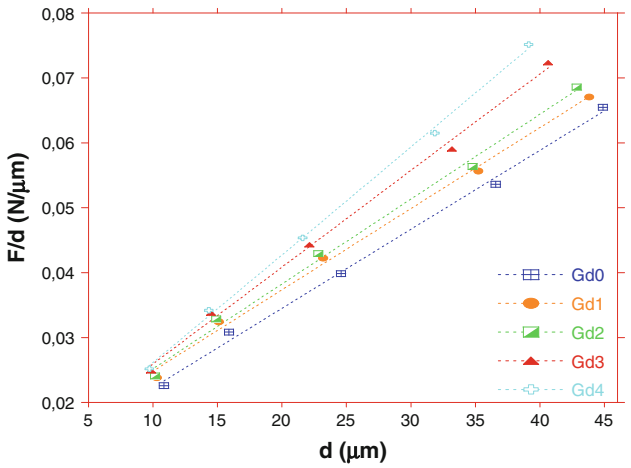

Fig. 7 Plots of *F/d* versus *d* for the samples

Table 4 Best-fit results of experimental data according to PSR model

Samples	$w \times 10^{-3}$ (N/μm)	$A \times 10^{-4}$ (N/μm)	H_{PSR} (GPa)	H_v (GPa)
Gd0	9.80	12.25	2.271	2.705–2.719
Gd1	12.01	12.57	2.330	2.842–2.932
Gd2	11.79	13.16	2.440	2.984–3.020
Gd3	10.66	14.99	2.779	3.310–3.315
Gd4	9.15	16.71	3.098	3.577–3.586

strength (Y_0), fracture toughness (K_{IC}) and brittleness index (B_0) and the results obtained are listed in Table 5. It is obvious from the figure that the H_0, E_0, Y_0 and B_0 values increase with the enhancement of the Gd concentration in the Y123 system. The increment in the Fracture toughness, being an important parameter for technological applications, is associated with the increase of the surface energy.

$$E = 81.9635H_V \tag{7}$$

$$Y \approx \frac{H_V}{3} \tag{8}$$

$$K_{IC} = \sqrt{2E\gamma} \tag{9}$$

$$B = \frac{H_v}{K_{IC}} \tag{10}$$

2.6.3 Analysis according to modified PSR (MPSR) model

MPSR model explaining the ISE behavior of the material [52] is defined with the aid of the following equation;

$$F = W_{MPSR} + A_{0MPSR}d + A_{1MPSR}d^2 \tag{11}$$

with respect to the MPSR model, the load independent microhardness value can be defined as:

$$H_{MPSR} = 1854.4A_{1MPSR} \tag{12}$$

Table 5 The calculated load independent H_0, E_0, Y_0 and K_{IC} for the samples

Samples	H_0 (GPa)	E_0 (GPa)	Y_0 (GPa)	K_{ic} (Pa/m$^{1/2}$)	H_v (GPa)
Gd0	2.271	186.13	0.757	1910.0	2.705–2.719
Gd1	2.330	190.97	0.776	2141.7	2.842–2.932
Gd2	2.440	199.99	0.813	2171.5	2.984–3.020
Gd3	2.779	227.77	0.926	2203.6	3.310–3.315
Gd4	3.098	253.92	1.032	2155.6	3.577–3.586

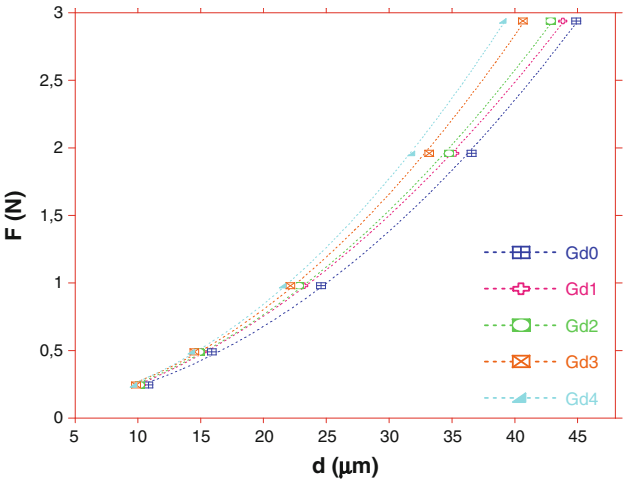

Fig. 8 Variation of applied load with the indentation diagonal length for the samples

The values of W_{MPSR}, A_{0MPRS}, A_{1MPRS} and H_{MPSR} deduced from *F–d* graph (Fig. 8) are listed in Table 6. As seen from table, for the Gd0 sample the H_{MPSR} value of 2.454 GPa computed by MPSR model is still lower than the H_v result in the plateau region (2.705 GPa). It is another important point observed from the table that the H_{MPSR} values calculated enhance with the increment of the Gd content.

2.6.4 Analysis according to elastic/plastic deformation (EPD) model

According to Upit et al. [53], the dependence of indentation size on the applied load is determined from the following equation:

$$F = A_2(d_e + d_p)^2 \tag{13}$$

where A_2 presents a constant, and d_e depends on the plastic deformation (d_p). The values of H_{EPD}, A_2 and d_e estimated from Fig. 9 are also illustrated in Table 7. Furthermore, the load independent microhardness (H_{EPD}) values are computed with the aid of the following equation:

$$H_{EPD} = 1854.4A_2 \tag{14}$$

Table 6 Best-fit results of experimental data according to MPSR model

Samples	W_{MPRS} (N)	A_{0MPRS} (N/μm)	A_{1MPRS} $\times 10^{-4}$ (N/μm^2)	H_{MPRS} (GPa)	H_v (GPa)
Gd0	0.06196	0.00435	13.236	2.454	2.705–2.719
Gd1	−0.01964	0.01469	11.993	2.223	2.842–2.932
Gd2	0.01469	0.01103	13.246	2.456	2.984–3.020
Gd3	0.05386	0.00557	15.987	2.964	3.310–3.315
Gd4	0.04630	0.00466	17.613	3.266	3.577–3.586

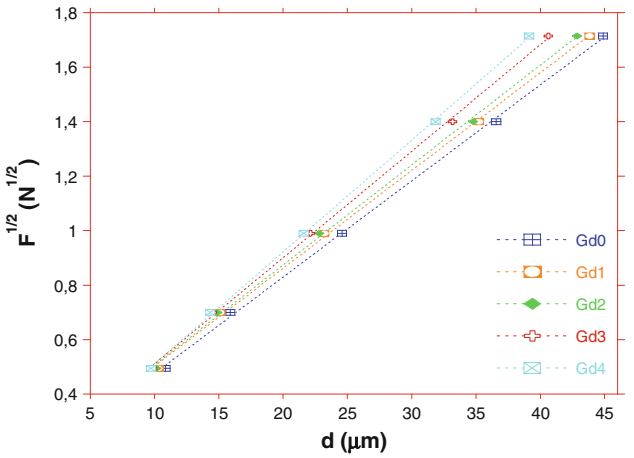

Fig. 9 Plots of square root of applied loads versus diagonal length for the samples

Table 7 Best-fit results of experimental data according to EPD model

Samples	A_2 (N/μm^2)	d_e (μm)	H_{EPD} (GPa)	H_V (GPa)
Gd0	0.0353	0.118	2.310	2.705–2.719
Gd1	0.0359	0.140	2.389	2.842–2.932
Gd2	0.0367	0.135	2.497	2.984–3.020
Gd3	0.0391	0.117	2.835	3.310–3.315
Gd4	0.0411	0.098	3.132	3.577–3.586

It is found that the H_{EPD} values obtained for the samples increase with enhancing the content of the Gd, similar to the case for Meyer's, PSR and MPSR models. As seen from Table 7, the calculated *de* values for all the samples prepared in this work are found to be positive, meaning that the elastic deformation is observed along with the plastic deformation. In other words, the presence of the elastic relaxation is observed for all the samples studied as a consequence of the ISE behavior.

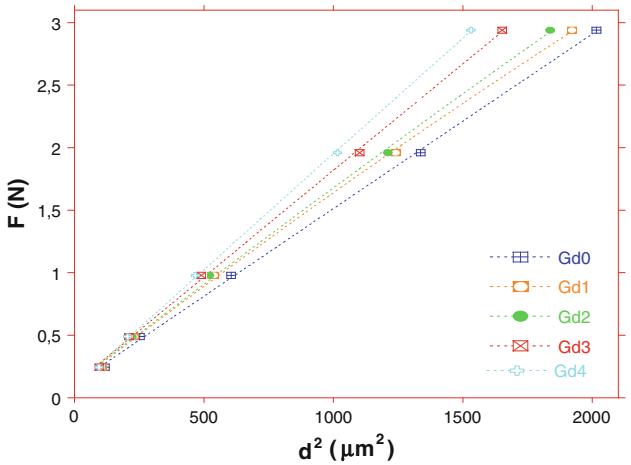

Fig. 10 Applied load versus the square of the impression length for the samples

2.6.5 *Analysis using Hays–Kendall approach*

Hays and Kendall proposed that there is minimum level of the applied test load (W_{HK}) to initiate plastic deformation. If the test load is not strong enough, only the elastic deformation in the system occurs. Thus, according to the Hays–Kendall (*HK*) report, the experimentally measured indentation size is proportional to an effective load $F_{eff} = F - W_{HK}$ rather than the applied load *F* [54].

$$F - W_{HK} = A_{1HK} d^2 \tag{15}$$

where A_{1HK} presents the load independent hardness constant The load independent microhardness can be explained by using the following equation:

$$H_{HK} = 1854.4 A_{1HK} \tag{16}$$

Figure 10 reveals the plots of *F* versus d^2 according to *HK* approach. It is apparent form the figure that all the curves obtained are linear for the samples. The slope of the line equals to the constant A_{1HK} when the intercept equals to the W_{HK}. The estimated best fit values of A_{1HK} and W_{HK} computed from Fig. 10 are listed in Table 8. One can see from the table that both the H_{HK} and A_{1HK} values increase with the enhancement of the Gd content in the Y123 system. It is another important point that all the W_{HK} values obtained are positive for the samples, meaning that the applied load is enough to create both the elastic and plastic deformation.

Among the models used in this work, the microhardness calculations obtained from HK model are found to be the closest to the values in the plateau (saturation) region for all samples displaying ISE behaviour (Table 8). Comparison between the H_{HK} values computed by HK approach (2.599 GPa) and the H_v results for the Gd0 sample in the plateau region (2.705 GPa) presents that the HK approach is the most successful model to define the hardness

Table 8 Best-fit results of experimental data according to HK model

Samples	A_{HK} (GPa) $\times 10^{-4}$	W_{HK} (N)	H_{HK} (GPa)	H_V (GPa)
Gd0	14.02	0.107	2.599	2.705–2.719
Gd1	14.66	0.137	2.718	2.842–2.932
Gd2	15.30	0.129	2.837	2.984–3.020
Gd3	17.09	0.107	3.169	3.310–3.315
Gd4	18.59	0.089	3.447	3.577–3.586

Table 9 The results of load dependent Vickers microhardness at the plateau region and load independent hardness values calculated using PSR, MPSR, EPD models and HK approach

Samples	H_{PSR} (GPa)	H_{MPRS} (GPa)	H_{EPD} (GPa)	H_{HK} (GPa)	H_V (GPa)
Gd0	2.271	2.454	2.310	2.599	2.705–2.719
Gd1	2.330	2.223	2.389	2.718	2.842–2.932
Gd2	2.440	2.456	2.497	2.837	2.984–3.020
Gd3	2.779	2.964	2.835	3.169	3.310–3.315
Gd4	3.098	3.266	3.132	3.447	3.577–3.586

mechanism of the samples produced. This behavior is also observed for the other samples (Gd1, Gd2, Gd3 and Gd4).

In this paper, we use five different models to examine the micro-indentation data on Gd doped bulk Y123 samples studied in this work. For comparison, the hardness results of the PSR, MPSR, EPD models and HK approach are given along with Vickers microhardness values of the samples in the plateau region in Table 9. It is apparent from the table that the Vickers microhardness values ascend with the increment of the Gd level in the system. The similar behaviour is observed for all the compared models. In summary, the load independent microhardness values calculated by HK approach give closer results to the ones in the plateau region when compared to the PSR, MPSR and EPD models, presenting that the Hays–Kendall (*HK*) approach is the most suitable method to analysis the mechanical properties of the $YBa_2Cu_{3-x}Gd_xO_{7-\delta}$ superconductors.

3 Conclusion

In the present work, we analyze the effect of partial replacement of Cu^{2+} ions by Gd^{+3} ions on the pinning mechanism, electrical, microstructural, physical, mechanical and superconducting properties of $YBa_2Cu_{3-x}Gd_xO_{7-\delta}$ superconductors. Vickers microhardness measurements are conducted to investigate the mechanical properties of the samples studied. Besides, the results of the microhardness measurements are examined using the different models such as Meyer's law, PSR, MPRS, EPD, and Hays-Kendall approach. Moreover, it is noted that the microstructural and superconducting properties of the samples are observed to depend strongly on the Gd content and the major findings to be obtained from this work are the following:

- The critical temperature values are found to reduce with the enhancement of the Gd-content in the Y123 system. Namely, the T_c^{onset} and T_c^{offset} values are obtained to be about 95.2 and 92.0 K for the Gd0 sample while the former and latter are observed to decrease to 93.6 and 83.3 K for Gd4 sample, respectively.
- SEM measurements indicate that the surface morphology of the Gd0 sample displays the most uniform surface appearance with largest grains, greatest crystallinity, lowest porosity, best texturing and connectivity between grains while the Gd4 sample with randomly oriented and poorly connected grains obtains the worst appearance among the samples. The decrement in the crystallite size is also favored by means of the grain size calculations of the XRD peaks.
- According to the XRD investigations, all the samples show the polycrystalline superconducting phase with less intensity of diffraction lines as the Gd content increases in the system and contain different phases such as Y123, Y211 and $BaCuO_2$. The peak intensities of the major phase (Y123) are obtained to reduce while the peak intensities belonging to minor phases ($BaCuO_2$ and Y211) are obtained to ascend methodically with the increment in the Gd addition, illustrating that Gd^{3+} ions are substituted by Cu^{2+} in the Y123 system successfully.
- The maximum J_c of 132 A/cm^2 is found for the Gd0 sample as against 34 A/cm^2 (minimum value) for the Gd4 sample. This suppression of J_c is associated with not only the reduction of the flux pinning centers but also the increase in the weak links between the superconducting grains, secondary phases, porosity, grain boundaries resistance and de-orientation of Y123 grains with the increment of the Gd content in the system.
- The Vickers hardness values obtained improve with the increment of the Gd doping into the Y123 system because of the enhancement in the strength of the bonds between grains.
- The results of the microhardness measurements are analyzed employing Meyer's law, PSR, MPSR, EDP models and Hays–Kendall approach. Hays–Kendall approach is found to be the best model to examine the mechanical properties of the bulk $YBa_2Cu_{3-x}Gd_xO_{7-\delta}$ superconductors.

References

1. M.K. Wu, J.R. Ashburn, C.J. Torng, Phys. Rev. Lett. **58**, 908 (1987)
2. P. Diko, Supercond. Sci. Technol. **13**, 1202 (2000)

3. A. Koblischka-Veneva, M.R. Koblischka, K. Ogasawara, M. Murakami, Cryst. Eng. **5**, 265 (2002)
4. K. Ogasawara, N. Sakai, M. Murakami, Supercond. Sci. Technol. **13**, 688 (2000)
5. C. Terzioglu, M. Yilmazlar, O. Ozturk, E. Yanmaz, Physica C **423**, 1190 (2005)
6. P.M. Sarun, S. Vinu, R. Shabna, A. Biju, U. Syamaprasad, Mater. Res. Bull. **44**, 1017 (2009)
7. Y. Feng, L. Zhou, J.G. Wen, N. Koshizuka, A. Sulpice, J.L. Tholence, J.C. Vallier, P. Monceau, Physica C **297**, 75 (1998)
8. L. Zhou, P. Zhang, P. Ji, K. Wang, X. Wu, Supercond. Sci. Technol. **3**, 390 (1990)
9. H. Fujimoto, M. Murakami, S. Dotoh, N. Koshizuka, S. Tanaka, Adv. Supercond. **2**, 285 (1990)
10. T. Egi, J.G. Wen, K. Koroda, H. Unoki, N. Koshizuka, Appl. Phys. Lett. **67**, 2406 (1995)
11. I. Felner, B. Brosh, Phys. Rev. B **43**, 10364 (1991)
12. C.W. Luo, Physica C **470**, 176 (2009)
13. T.D. Dzhafarov, M. Altunbas, A. Varilci, U. Cevik, A.I. Kopya, Mater. Lett. **26**, 305 (1996)
14. T.D. Dzhafarov, U. Cevik, J. Mater. Sci. Mater. Electron. **12**, 193 (2001)
15. H. Eisaki, N. Kaneko, D.L. Feng, A. Damascelli, P.K. Mang, K.M. Shen, Z.X. Shen, M. Greven, Phys. Rev. B **69**, 064512 (2004)
16. K. Fujita, T. Noda, K.M. Kojima, H. Eisaki, S. Uchida, Phys. Rev. Lett. **95**, 097006 (2005)
17. S.B. Guner, O. Gorur, S. Celik, M. Dogruer, G. Yildirim, A. Varilci, C. Terzioglu, J. Alloy. Compd. (2012). doi:10.1016/j.jallcom.2012.06.082
18. K. Ozturk, S. Celik, U. Cevik, E. Yanmaz, J. Alloy. Compd. **433**, 46 (2007)
19. N.P. Liyanawaduge, S.K. Singh, A. Kumar, V.P.S. Awana, H. Kishan, J. Supercond. Nov. Magn. **24**, 1599 (2011)
20. R. Lal, S.P. Pandey, A.V. Narlikar, Phys. Rev. B **49**, 6382 (1994)
21. X.S. Wu, S.S. Jiang, C.C. Lam, D.W. Wang, X.L. Huarg, Z.H. Wu, Y. Yuan, X. Jin, Phys. Status Solidi A **157**, 439 (1996)
22. M.A. Ansari, R. Nigam, V.P.S. Awana, A. Gupta, R.B. Saxena, H. Kishan, N.P. Lalla, V. Ganesan, A.V. Narlikar, C.A. Cardoso, J. Appl. Phys. **97**, 10B104 (2005)
23. G. Yildirim, S. Bal, E. Yucel, M. Dogruer, M. Akdogan, A. Varilci, C. Terzioglu, J. Supercond. Nov. Magn. **25**, 381 (2012)
24. A. Ianculescu, M. Gartner, B. Despax, V. Bley, T.H. Leby, R. Gavrila, M. Modreanu, Appl. Surf. Sci. **253**, 344 (1996)
25. S. Vinu, P.M. Sarun, A. Biju, R. Shabna, P. Guruswamy, U. Syamaprasad, Supercond. Sci. Technol. **21**, 045001 (2008)
26. R. Shabna, P.M. Sarun, S. Vinu, A. Biju, U. Syamaprasad, Supercond. Sci. Technol. **22**, 045016 (2009)
27. H. Wang, A. Serquis, B. Maiorov, L. Civale, Q.X. Jia, P.N. Arendt, S.R. Foltyn, J.L. Macmanus-Driscoll, X. Zhang, J. Appl. Phys. **100**, 053904 (2006)
28. P.M. Sarun, S. Vinu, R. Shabna, A. Biju, U. Syamaprasad, J. Alloy. Compd. **472**, 13 (2009)
29. R. Shabna, P.M. Sarun, S. Vinu, A. Biju, U. Syamaprasad, J. Alloy. Compd. **493**, 11 (2010)
30. A. Biju, P.M. Sarun, R.P. Aloysius, U. Syamaprasad, J. Alloy. Compd. **454**, 46 (2008)
31. G. Yildirim, A. Varilci, M. Akdogan, C. Terzioglu, J. Mater. Sci. Mater. Electron **23**, 928 (2012)
32. M. Dogruer, G. Yildirim, E. Yucel, C. Terzioglu, J. Mater. Sci. Mater. Electron. (2012). doi:10.1007/s10854-012-0689-6
33. M. Dogruer, G. Yildirim, O. Ozturk, C. Terzioglu, J. Supercond. Nov. Magn. (2012). doi:10.1007/s10948-012-1719-6
34. S. Bal, M. Dogruer, G. Yildirim, A. Varilci, C. Terzioglu, Y. Zalaoglu, J. Supercond. Nov. Magn. **25**, 847 (2012)
35. A. Tampieri, G. Celotti, S. Lesca, G. Bezzi, T.M.G. La Torretta, G. Magnani, J. Eur. Ceram. Soc. **20**, 119 (2000)
36. A. Biju, R.P. Aloysius, U. Syamaprasad, Supercond. Sci. Technol. **18**, 1454 (2005)
37. M. Tachiki, S. Takahashi, Solid State Commun. **70**, 291 (1989)
38. M. Tachiki, S. Takahashi, Solid State Commun. **72**, 1083 (1989)
39. A.I. Abou-Aly, S.A. Mahmoud, R. Awad, M.M.E. Barakat, J. Supercond. Nov. Magn. **23**, 1575 (2010)
40. H.C. Ling, M.F. Yan, J. Appl. Phys. **64**, 1307 (1988)
41. E. Asikuzun, O. Ozturk, H.A. Cetinkara, G. Yildirim, A. Varilci, M. Yılmazlar, C. Terzioglu, J. Mater. Sci. Mater. Electron. **23**, 1001 (2012)
42. M. Yilmazlar, O. Ozturk, O. Gorur, I. Belenli, C. Terzioglu, Supercond. Sci. Technol. **20**, 365 (2007)
43. H. Li, R.C. Bradt, J. Mater. Sci. **22**, 917 (1993)
44. C. Hays, E.G. Kendall, Metallography **6**, 275 (1973)
45. M. Dogruer, O. Gorur, Y. Zalaoglu, O. Ozturk, G. Yildirim, A. Varilci, C. Terzioglu, J. Mater. Sci. Mater. Electron. (2012). doi:10.1007/s10854-012-0755-0
46. J. Gong, J. Wu, Z. Guan, J. Eur. Ceram. Soc. **19**, 2625 (1999)
47. C. Terzioglu, J. Alloy. Compd. **509**, 87 (2011)
48. R. Tickoo, R.P. Tandon, K.K. Bamzai, P.N. Kotru, Mater. Chem. Phys. **42**, 446 (2003)
49. A.A. Elmustafa, D.S. Stone, J. Mech. Phys. Solid. **51**, 357 (2003)
50. S.M. Khalil, J. Phys. Chem. Solids **62**, 457 (2001)
51. O. Ozturk, E. Asikuzun, M. Erdem, G. Yildirim, O. Yildiz, C. Terzioglu, J. Mater. Sci. Mater. Electron. **23**, 511 (2012)
52. J.B. Quinn, V.D. Quinn, J. Mater. Sci. **32**, 4331 (1997)
53. G.P. Upit, S.A. Varchenya, Phys. Status Solidi A **17**, 831 (1966)
54. M. Ozturk, E. Erdem, O. Asikuzun, G. Yildiz, A. Yildirim, C. Varilci, J. Terzioglu, Mater. Sci Mater. Electron. (2012). doi:10.1007/s10854-012-0722-9